Nanoscale

Accepted Manuscript

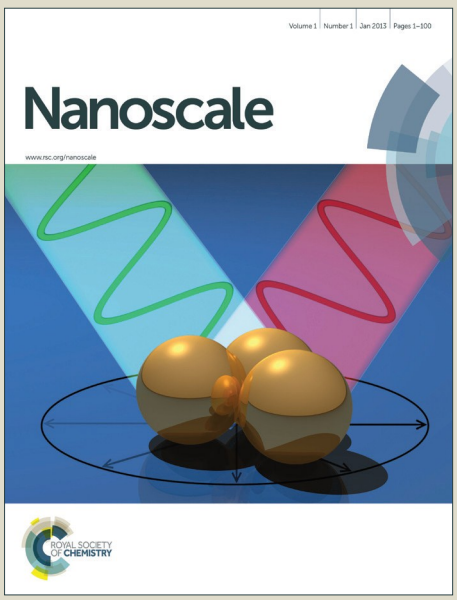

ROYAL SOCIETY OF CHEMISTRY

www.rsc.org/nanoscale

Nanosized graphene crystallite induced strong magnetism in pure carbon films

Chao Wang, Xi Zhang, Dongfeng Diao*

Institute of Nanosurface Science and Engineering, Shenzhen University,

Shenzhen 518060, China

Abstract:

We report strong magnetism in pure carbon films grown by electron irradiation assisted physical vapor deposition in electron cyclotron resonance plasma. The development of graphene nanocrystallite in amorphous film matrix, and the dependence of the magnetic behavior on amorphous, nanocrystallite and graphite like structures were investigated. Results were that amorphous structure shows weak paramagnetism, graphene nanocrystallite leads to strong magnetization, and graphite like structure corresponded with a lower magnetization. At room temperature of 300 K, the highest saturation magnetization of 0.37 emu/g was found in nanosized graphene nanocrystallite structure. The origin of strong magnetism in nanocrystallite was ascribed to the spin magnetic moment at graphene layer edges.

*Corresponding author. Tel. Fax: +86 0755 26902415.
E-mail address: dfdiao@szu.edu.cn (D. Diao)

1. Introduction

Carbon based nano devices have bright prospects in modern semiconductor industry since they can be easily integrated with silicon substrate during fabrication, and they can effectively reduce resource and energy consumptions. Nano devices derived from carbon material such as graphene [1] and carbon nanotubes [2] have shown significant performances. Recently, nanocrystallite-contained carbon films attracted much attention owing to their unique mechanical [3], optical [4], electrical [5] and other properties. They can also be expected as candidates for novel carbon based nano devices.

Other than the mentioned properties, magnetism in pure carbon materials [6-11] have stimulated extensive studies to search for novel metal-free magnetic devices. Magnetic behaviors have been found in various carbon allotropies such as C_{60} [6], carbon nanofoam [7], nanofibers [8], irradiated graphite [9, 10] and nanodiamond [11]. The prediction of magnetism derived from graphene [12] is particularly intriguing, since graphene is considered as the basis for next generation electronic and spintronics devices [13]. Researches on magnetism originated in graphene oxide [14], graphene nanoflakes [15, 16], hydrogenated graphene [17] and graphene nanoribbons [18] suggested that the magnetic behavior of graphene based materials is in a large part governed by their edge structures. Even in carbon-nitrogen compound, the magnetism also originated from unpaired carbon atoms at edge defects [19]. Although the mechanism of carbon magnetism is complicated and can be divergent due to different atomic configurations [20-24], theoretical researches have demonstrated that orderly arrangement of spin magnetic moment at graphene layer edge is an important source for carbon magnetism, which can be in various types [25,26]. However, the existing approaches for magnetic carbon films need a second step of treatment to induce magnetism, and the one-

step preparation methods only can produce dispersed particles or flakes, the direct growth of strong-magnetic carbon films in a productive manner is still a challenge. Recent-discovered magnetism in graphene layer embedded carbon films [27] showed that higher magnetization can be expected if the content of graphene nanocrystallite further increased. Since low energy electron irradiation in plasma-assisting deposition has been found capable to modulate the nanocrystallite formation [28, 29], it is an effective way to modify the magnetic behaviors of pure carbon film by controlling film structures.

In this study, we used low energy electron irradiation in electron cyclotron resonance (ECR) plasma to induce graphene nanocrystallite formation and development in carbon films, thus modulating the film magnetic behaviors. Different electron irradiation densities and energies were employed by altering gas pressure and substrate bias voltage, respectively. The film structures and graphene layer edge development were characterized by transmission electron microscopy (TEM) observation together with Raman spectra analysis. The saturation magnetization, temperature-dependence of magnetization, and electric resistivity of the films were measured. The types and origins of magnetism in different film structures were recognized by temperature-dependence measurement of magnetization.

2. Experimental details

Film deposition was carried out in an ECR plasma sputtering system, in which the low energy electron irradiation technique was introduced in argon plasma. The realization of electron irradiation was introduced in figure S1 in supplementary materials [30]. The carbon films were grown on silicon (100) surface, and the substrate size was $20\times20\times0.5$ mm^3. Before film deposition, the silicon wafer was cleaned in acetone and ethanol bath successively by ultrasonic wave, then was fixed onto the substrate holder and put into the vacuum chamber.

The vacuum chamber was pumped down to base vacuum of 3×10^{-4} Pa, then argon gas was inflated to generate plasma. When plasma was stabilized, the substrate surface was firstly cleaned by argon ion at the bias voltage of -50 V for 3 minutes. Thereafter, a sputtering bias voltage of -300 V was applied onto carbon target to generate carbon atoms for film growth. During film growth, low electron irradiation was introduced in order to induce graphene layer growth. In this study, electron irradiation density varied from 10^{10} cm^{-3} to 1.5×10^{11} cm^{-3}, and irradiation energy varied from 0 eV to 300 eV. The depositing time was 15min and the substrate temperature rose from room temperature to less than 200 °C during the deposition process, which was measured by thermometer.

The structures of carbon films were observed using JEOL-2010 TEM with the electron acceleration voltage of 300 kV. Plan view TEM specimens were prepared by scraping the film from Si substrate and transferring the flakes onto copper micro grid. The bonding structures of the films were studied from their Raman spectra, which were obtained with HORIBA HR800 laser confocal Raman spectrometer. The 514 nm laser spot size was 2 μm using a 100× objective, and the laser power was kept at 0.1 mW to avoid sample surface heating. The electric resistivity of the films was measured using four-probe-method, and the saturation magnetizations were obtained from a Superconductivity Quantum Interference Device (SQUID) at constant temperature of 300 K with magnetic field intensity between ±10 kOe. Field cooling (FC) and Zero field cooing (ZFC) test was carried out from 3 to 370 K under the magnetic field of 500 Oe.

3. Results and discussion

With electron irradiation energies varied from 10 to 300 eV, different structures were carbon films showed different structures as exhibited in figure 1, where Raman spectra,

electric resistivities and TEM images are listed from (a) to (d). With the irradiation energy of 10 eV, the Raman spectrum showed a broad band from 1100 cm^{-1} to 1800 cm^{-1}, with no 2D band detected (labeled as A in blue color), both features indicating an amorphous structure, as shown in figure 1 (a). When irradiation energy was between 40 and 300 eV, the Raman spectra contain separable D and G bands around 1340 cm^{-1} to 1580 cm^{-1}. The clear-shaped D band representing the long range ordered structure with sp^2 hybridization in amorphous structure. The 2D band also appear in these spectra, suggesting the existence of graphene layers since it arise from the two-phonon involved double resonance Raman process, which typically occurs inside graphene layer [31]. The increase of 2D band intensity from 40 to 150 eV is another proof for the increasing amount of graphene layers in the films. We refer the structure with the above Raman features as nanocrystallite structure, and the films with irradiation energies of 50 and 150 eV were labeled as sample B (red) and C (violet), respectively. When irradiation energy further increased from 200 eV to 300 eV, the 2D band gradually reduced, which was attributed to the formation of graphite-like structure in the film, where edge defects were less than in the former nanocrystallite contained structure. The film with irradiation energy of 200 eV was labeled as D (green). The D/G band ratio I_D/I_G for each spectrum was obtained by Breit-Wigner-Fano (BWF) fitting [32], and the results are shown in figure 1 (b), together with the film resistivity. It is clear that for from amorphous (A) to nanocrystallite structure (B), the I_D/I_G value showed a steep increment from 0.4 to 1.2, which further confirmed the formation of nanocrystallite [33]. The film electric resistivity suddenly dropped by one order of magnitude due to the formation of graphene nanocrystallite, which were more conductive than amorphous structure. The structural change from nanocrystallite (C) to graphite-like (D) can be seen from the reduction of both I_D/I_G ratio and electric

resistivity, and barely changed after irradiation energy higher than 200 eV, since the structure remained graphite-like in those cases.

In our research, the 2D band shape evolved with different film structures, and the change can be clearly described by Lorentz fitting results, as shown in figure 1 (b). For amorphous structure (A), no 2D band was detected. For graphene nanocrystallite structure (from B to C), the 2D bands are precisely fitted with four Lorentz components, representing an electronic structure similar to bilayer graphene [28, 34, 35]. For graphite-like structure, more than four components are needed to fit the 2D band, because more peaks appeared at the band shoulders, indicating more complicated electronic structure than bilayer graphene due to the merging of graphene layer edges between nano crystallites. This feature of 2D band can be helpful in our study to identify whether the film is nanocrystallite structure or graphite-like structure.

Different film structures can be seen in TEM images in figure 1 (d). For sample A, the TEM mage showed amorphous structure, with no graphene layers observed in the film. For sample B, small sized graphene nanocrystallites can be seen, each containing several graphene layers, and the graphene layer showed twisting and curving. For sample C, more graphene nanocrystallites were found, while no obvious difference from sample B was seen. For sample D, instead of small sized nano crystallite, bulk graphite-like structure with orderly aligned graphene layers can be seen. The lateral size of graphene layer became larger, and the graphene layer stacks connected with each other, which lead to less graphene layer edges between stacks. Due to our TEM observation, the nano crystallites and graphene layers existed not only in the figure showed area, but also in the whole film. From above results, we can see that the TEM images and Raman spectra keep good agreement in telling the

differences between amorphous, nanocrystallite and graphite like structures. When irradiation energy was between 50 and 150 eV, graphene layer edges gradually increased due to the increase of small sized few layer graphene stacks, and with irradiation energy larger than 200 eV, the film structures were still graphite like, which can be seen from TEM images in figure S2[30].

The magnetic behaviors of the films were measured with a SQUID MPMS-XL-7 from Quantum Design at the constant temperature of 300 K, which is the most probable temperature in real application atmosphere. During measurement, the effect of magnetic contamination was negligible according to plasma mass spectrometry test on the impurity element concentrations [30]. For each measurement, the magnetic field was applied from 0 to +10 kOe, then changed from +10 kOe to -10 kOe, and finally went back to 0, hence a hysteresis loop was obtained. Different changing rates of magnetic field were employed, which increased from 0.02(-0.1 to +0.1 kOe) to 0.5 (±3 to ±10 kOe). This sampling method was used in order to shorten the measuring process and detailed information also can be seen at lower magnetic field range. The magnetization curves (M-H curves) of sample A-D are shown in figure 2 (a), where different saturation magnetizations Ms can be seen. For amorphous structure with no graphene layers edge (sample A), M_s was 0.017 emu/g. When graphene layer edges were formed (sample B), M_s increased to 0.075 emu/g. When more graphene nanocrystallites were produced in the film (sample C), M_s further increased to 0.27 emu/g. When graphite like structure was formed (sample D), M_s decreased to 0.12 emu/g. Figure 2 (b) presented the hysteresis loops in a smaller magnetic field region, in which the change of residual magnetism Br can be seen more clearly (Detail values were plotted in table S2 [30]). Like the saturation magnetization, M_r value increased when amorphous structure (A)

changed into nanocrystallite structure (B), and reached maximum (C) before film structure further change into graphit like (D).

A similar relationship between magnetization and the development of film structure was also noticed when film growth was carrying out under the electron irradiation density of 10^{10} cm^{-1}. The magnetic measurement results were shown in figure 2 (c), where the increasing of M_s can be clearly seen as the increasing of graphene nanocrystallites. Amorphous structure was obtained at the irradiation energy of 10 eV (sample E), and the magnetization was 0.008 emu/g. Small sized nanocrystallite appeared at the energy of 50 eV (sample F), with the magnetization rose to 0.04 emu/g. The film magnetization reached to maximum of 0.37 emu/g at 250eV (sample G), larger than recently reported room temperature magnetization in pure-carbon allotropes [14-17, 36, 37]. When structure changed into graphite like at 300 eV (sample H) and the magnetization reduced to 0.14 emu/g. Comparing with figure 2 (b), the hysteresis loops in figure 2 (d) also clearly showed that the nanocrystallite structure can possess larger residual magnetism when grown under lower irradiation density. Although the irradiation energies for achieving maximum M_s are different, it is quite evident that the increase of graphene nanocrystallites can lead to strong magnetism and graphite like structure are less "magnetic" than graphene nanocrystallite structure.

In order to further recognize the magnetic properties of the films, field cooling (FC) and zero-field cooling (ZFC) measurements were carried out for of amorphous structure (sample E) and nanocrystallite structure (sample G) at 500 Oe, and different types of temperature dependence were found, as shown in figure 3. The background diamagnetic signals form plastic foils and capsules have been subtracted. For amorphous structure, the FC curve (red)

and ZFC curve (blue) almost coincided with each other as shown in figure 3 (a), and exhibited weak paramagnetic behavior. The slight divergence may come from the free spins which are of very low concentration in amorphous carbon base. On the other hand, a clearer separation can be seen between the FC and ZFC curves for nanocrystallite structure, in the temperature range of 350 K to 250 K, where the ZFC curve reached its maximum value. The maximum point of ZFC curve can usually represent the blocking temperature of a magnetic system [38-41], however, the size of graphene nanocrystallite are not exactly the same, so the blocking temperature may be different since the size of "magnetic particle" can influence the blocking temperature. We think that is why the curves did not clearly show a separation at 250 K where the ZFC curve reached its maximum value. Actually, we tend to believe the vibration of blocking temperature ranges from 250 K to 350 K, where the separation starts. From 250K to 30K, the FC curve showed a trend of decreasing of magnetization and at low temperature (less than 30 K), the paramagnetic behavior of amorphous matrix of the film is still detectable. However, the magnetism originated from nanocrystallite is predominant during most of the measurement. Therefore, the strong carbon magnetism in our study is mainly ascribed to the nanocrystallite structure. Furthermore, we already found that the magnetism will become weaker for graphite-like structure that contains larger graphene layers than nanorystallite structure did. Therefore, strong magnetism are more possibly originated from the graphene layer edges, which are more concentrated in nanocrystallite structure than in graphite like structure, and increase proportionate with the formation of nanocrystallites.

In the aim of revealing the relationship between graphene layer edges and magnetic behaviors, more carbon films were deposited under different electron irradiation densities and energies, with the density range expanded to 10^{10} - 1.5×10^{11} cm^{-3}, and energy range 10 - 350

eV. Electron irradiation with density lower than 10^{10} cm^{-3} could not be realized in our study since plasma was not stable under such low density, and for irradiation density of 1.5×10^{11} cm^{-3}, the electron current density will reach to the equipment limitation when irradiation energy was higher than 150 eV. Saturation magnetization values and electric resistivities were measured for each film, and their structures were observed focusing on the nanocrystallite size and formations. The overall results were summarized in figure 4 as a structure-magnetization diagram of the magnetic carbon film. The samples near the boundaries between different structures were listed from A to J. The electric resistivity and saturation magnetization of each sample were also labeled in the figure.

The diagram clearly showed that strong magnetization can be obtained in the region where nanocrystallite structure can be obtained. For same electron irradiation density, the highest magnetization was achieved when graphene nanocrystallites were mostly yielded before graphite-like structure was formed. The diagram also showed that lower irradiation density was beneficial for stronger magnetism. This is because that higher irradiation energy can be reached in lower electron irradiation density before graphite-like structure formation, thus leading to high content of nanocrystallites.

On the other hand, the film electrical resistivity was not determined by graphene layer edges. Instead, it showed a clearly dependence on the graphene layer content. For same irradiation density, the resistivity value drops for one order of magnitude with the change from amorphous to nanocrystallite strucutre, and nanocrystallite to graphite like structure. So it can be inferred that the electric property was governed by the amount and size of graphene layers rather than graphene layer edges.

Figure 5 summarized the changing tendencies of resistivity and saturation magnetization

along with different film structures. As exhibited in the figure, graphene nanocrystallite can bring about larger magnetization than other structures. The structural evolving from graphene nanocrystallite to graphite-like structure leads to better electric performance but at the same time results in lower magnetization. The figure also suggests that lower electron irradiation density is preferred to obtain strong magnetization for nanocrytallite structure since larger amount of nanocrystallites are yielded. So for magnetic and spintronics applications, it is necessary to produce more nanosized graphene crystallites, so that graphene layer edges are abundant in carbon films.

Our related simulation works have confirmed that the undercoordinated carbon atoms at graphene layer edges can trap net spin moment, which lead to strong magnetic behaviors [42]. So the spin at the graphene layer edges may be the origin of the strong magnetic interactions in this research. From TEM and Raman observations, we note that the structural transition of sample A-D and E-H follow the order of: amorphous, nanocrystallite, abundant nanocrystallite and graphite-like. Magnetic measurement revealed that strong magnetism were achieved in sample C and G, which are in the “abundant nanocrystallite” stage, and graphene layer edges are mostly produced at this stage. So we suggested that the origin of the strong magnetism may come from the graphene layer edges.

4. Conclusion

In order to explore strong magnetism in pure carbon films and recognize the role of graphene layer edges on film magnetic behaviors, we performed low energy electron irradiation to modulate graphene nanocrystallite development in film deposition. Pure carbon films with amorphous, nanocrystallite and graphite like structures were obtained.

Magnetization studies showed that by increase the amount of graphene nanocrystallite, the film magnetization can achieve 0.37 emu/g from 0.008 emu/g. Hysteresis loops and FC/ZFC measurements confirmed the strong magnetic behavior of graphene nanocrystallite. The origin of strong magnetism of the film was derived from spin magnetic moment at graphene layer edges in nanosized cystallites. A diagram of structure-magnetization evolution was proposed, and the fact was found that small size nanocrystallites with are beneficial for strong magnetization since they provide large amount of graphene layer edges. This research brings about an effective way to fabricate pure carbon films with strong magnetism, which is a candidate for potential applications in spintronics and nano electromechanical systems.

Acknowledgement

The authors thank the National Nature Science Foundation of China with Grant Numbers of 51305274, 91323303, as well as the Young-Researcher-Starting Grant of Shenzhen University (201442).

References

[1] F. Schwierz, *Nature Nanotech.*, 2010, **5**, 487.

[2] T. Yamada, Y. Hayamizu, Y. Yamamoto, Y. Yomogida, A. Izadi-Najafabadi, D. N. Futada, D. N. Futaba and K. Hata, *Nature Nanotech.*, 2011, **27**, 296.

[3] D. W. M. Lau, D. G. McCulloch, M. B. Taylor, J. G. Partridge, D. R. McKenzie, N. A. Marks, E. H. T. Teo and B. K. Tay, *Phys. Rev. Lett.*, 2008, **100**, 176101.

[4] M. Shakerzaheh, N. Xu, M. Bosman, B. K. Tay, X. Wang, E. H. T. Teo, H. Zheng and H. Yu, *Carbon*, 2011, **49**, 1018.

[5] Y. Chen, H. Medina, H. Tsai, T. Su, H. Lin and Y. Chueh, *Nanoscale*, 2014, DOI: 10.1039/C4NR04627G.

[6] T. L. Makarova, B. Sundqvist, R. Hohne, P. Esquinazi, Y. Kopelevich, P. Scharff, V. A. Davydov, L. S. Kashevarova and A. V. Rakhmanina, *Nature*, 2001, **413**, 716.

[7] A. V. Rode, E. G. Gamaly, A. G. Christy, J. G. F. Gerald, S. T. Hyde, R. G. Elliman, B. Luther-Davies, A. I. Veinger, J. Androulakis and J. Giapintzakes, *Phys. Rev. B*, 2004, **70**, 054407.

[8] S. Ma, J. H. Xia, V. V. S. S. Srikanth, X. Sun, T. Staedler, X. Jiang, F. Yang and Z. D. Zhang, *Appl. Phys. Lett.*, 2009, **95**, 263105.

[9] P. Esquinazi, D. Spemann, R. Hohne, A. Setzer, K. H. Han and T. Butz, *Phys. Rev. Lett*., 2003, **91**, 227201.

[10] O. V. Yazyev, *Phys. Rev. Lett.*, 2008, **101**, 037203.

[11] S. Talapatra, P. G. Ganesan, T. Kim, R. Vajtai, M. Huang, M. Shima, G. Ramanath, D. Srivastava, S. C. Deevi and P. M. Ajayan, *Phys. Rev. Lett.*, 2005, **95**,097201.

[12] Y. W. Son, M. L. Cohen, S. G. Louie, *Nature*, 2006, **444**, 347.

[13] O. V. Yazyev, M. L. Katsnelson, *Phys. Rev. Lett.*, 2008, **100**, 047209.

[14] Y. Wang, Y. Huang, Y. Song, X. Zhang, Y. Ma, J. Liang and Y. Chen, *Nano Lett.*, 2009, **9**, 220.

[15] A. Ney, P. Papakonstantinou, A. Kumar, N. G. Shang, N. Peng, *Appl. Phys. Lett.*, 2011, **99**, 102504.

[16] C. S. Rout, A. Kumar, N. Kumar, A. Sundaresan and T. S. Fisher, *Nanoscale*, 2011, **3**, 900.

[17] L. Xie, X. Wang, J. Lu, Z. Ni, Z. Luo, H. Mao, R. Wang, Y. Wang, H. Huang, D. Qi, et al., *Appl. Phys. Lett.*, 2011, **98**, 193113.

[18] G. Z. Magda, X. Jin, I. Hagymasi, P. Vancso, Z. Osvath, P. Nemes-Incze, C. Hwang, L.

P. Biro and L. Tapaszto, *Nature*, 2014, **514**, 608.

[19] D. Gao, Q. Xu, J. Zhang, Z. Yang, M. Si, Z. Yan, M. Su, Z. Yan and D. Xue, *Nanoscale*, 2014, **6**, 2577.

[20] Y. W. Son, M. L. Cohen and S. G. Louie, *Phys. Rev. Lett.*, 2006, **97**, 216803.

[21] H. Santos, A. Ayuela, L. Chico and E. Artacho, *Phys. Rev. B*, 2012, **85**, 245430.

[22] M. J. Schmidt, D. Loss, *Phys. Rev. B*, 2010, **82**, 085422.

[23] W. Li, M. Zhao, Y. Xia, R. Zhang and Y. Mu, *J Mater. Chem.*, 2009, **19**, 9274.

[24] R. R. Nair, M. Sepioni, I-Ling Tsai, O. Lehtinen, J. Keinonen, A. V. Krasheninnikov, T. Thomson, A. K. Geim and I. *V, Nat. Phys.*, 2012, **8**, 199.

[25] H. Feldner, Z. Y. Meng, T. C. Lang, F. F. Assaad, S. Wessel and A. Honecker, *Phys. Rev. Lett.*, 2011, **106**, 226401.

[26]M. Golor, S. Wessel and M. J. Schmidt, *Phys. Rev. Lett.*, 2014, **112**, 046601.

[27] C. Wang and D. Diao, *Appl. Phys. Lett.*, 2013, **102**, 052402.

[28] C. Wang, D. Diao, X. Fan and C. Chen, *Appl. Phys. Lett*., 2012, **100**, 231909.

[29] C. Wang and D. Diao, *Surf. Coat. Technol.*, 2011, **206**, 1899-1904.

[30] See supplementary materials for detailed description of low energy electron irradiation technique, more TEM images of carbon films deposited under different electron irradiation energies and plasma mass spectrometry test results.

[31] L. M. Malard, M.A. Pimenta, G. Dresselhaus, M.S. Dresselhaus, *Phys. Rep.*, 2009, **473**, 51.

[32] S. D. M. Brown, A. Jorio, P. Corio, M. S. Dresselhaus, G. Dresselhaus, R. Saito and K. Kneipp, *Phys. Rev. B*, 2001, **63**, 155414.

[33] A. C. Ferrari, J. Robertson, *Phys. Rev. B*, 2000, **61**, 14095.

[34] A. C. Ferrari, J. C. Meyer, V. Scardaci, C. Casiraghi, M. Lazzeri, F. Mauri, S. Piscanec, D. Jiang, K. S. Novoselov, S. Roth, et al., *Phys. Rev. Lett.*, 2006, **97**, 187401.

[35] M. Okano, R. Matsunaga, K. Matsuda, S. Masubuchi, T. Machida and Y. Kanemitsu, *Appl. Phys. Lett.*, 2011, **99**, 151916.

[36] S. Qin, X. Guo, Y. Cao, Z. Ni and Q. Xu, *Carbon*, 2014, **78**, 559.

[37] H. S. S. Ramakrishna Matte, K. S. Subrahmanyam and C. N. R. Rao, *J Phys. Chem. C*, 2009, **113**, 9982.

[38] A. Ludwig, L. Agudo, G. Eggeler, L. Ludwig, A. D. Wieck and O. Petracic, *Appl. Phys. Lett.*, 2013, **113**, 043917.

[39] J. T. Abiade, S. H. Oh, D. Kumar, M. Varela, S. Pennycook, H. Guo, A. Gupta and J. Sankar, *Appl. Phys. Lett.*, 2008, **104**, 073910.

[40] M. Knobel, W. C. Nunes, H. Winnishofer, T. C. R. Rocha, L. M. Socolovsky, C. L. Mayorga and D. Zanchet, *J Non-Cryst. Solids*, 2007, **353**, 743.

[41] H. Mamiya. M. Ohnuma, I. Nakatani and T. Furubayashim, *IEEE T. Magn.*, 2005, **41**, 3394.

[42] X. Zhang, C. Wang, C. Q. Sun and D. Diao, *Appl. Phys. Lett.*, 2014, **105**, 042402.

Figure Captions

Figure 1. (a) Raman spectra of carbon films with different electron irradiation energies from 10 to 300 eV under the irradiation density of 10^{11} cm^{-3}. The spectra at 10, 50,150 and 200 eV were labeled as A (red), B (blue), C (violet); and D (green), revealing the films of different structures. (b) Detailed spectra between 2500 cm^{-1} and 2800 cm^{-1}, where 2D bands of sample B, C, D were pointed out. (c) The D band and G band ratios obtained from the Raman spectra of the films as well as their electrical resistivities. (d) Plan-view TEM images of sample A-D and their electron diffraction patterns.

Figure 2. Magnetization curves of carbon films with different structures at the temperature of 300 K. Diamagnetic signals from plastic foils and capsules have been subtracted. The magnetization results for sample A-D are plotted in (a) with solid squares. The hysteresis loops in smaller magnetic field region are plotted in (b) with hollow squares. When electron irradiation density reduced for an order of magnitude, the films with different structures were obtained, which were listed as sample E-G. The magnetization results for sample E-G are plotted in (c) with solid circles, and the hysteresis loops are plotted in (d) with hollow circles.

Figure 3. FC-ZFC curves of (a) amorphous (sample E) and (b) nanocrystallite structure (sample G) under applied magnetic field of 500 Oe. The diamagnetic signals from background have been subtracted.

Figure 4. The structure-magnetization diagram of magnetic carbon film as the function of electron irradiation energy and density. Electric resistivity was labeled in the unit of Ω·cm, followed by saturation magnetization in the unit of emu/g. The grey region in the figure

means film could not be obtained so far due to current equipment limitation in our study.

Figure 5. Resistivity and magnetization changing tendencies of carbon films along with different film structures.

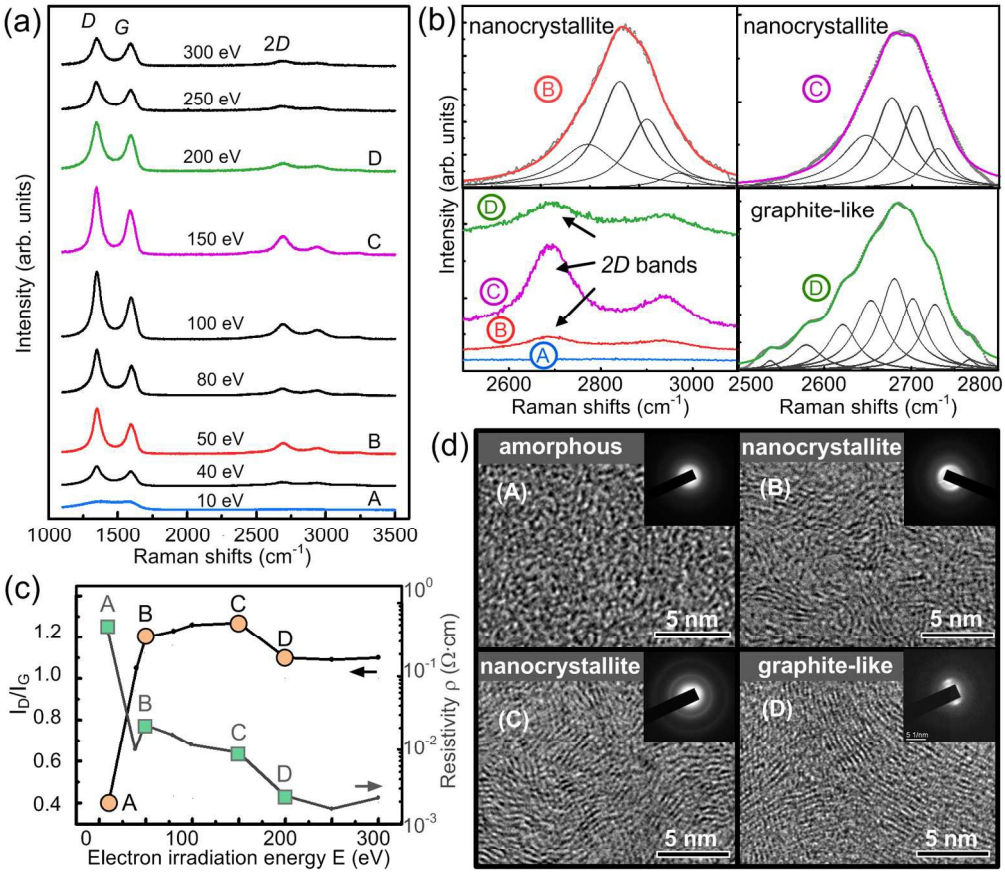

Figure 1

155x148mm (300 x 300 DPI)

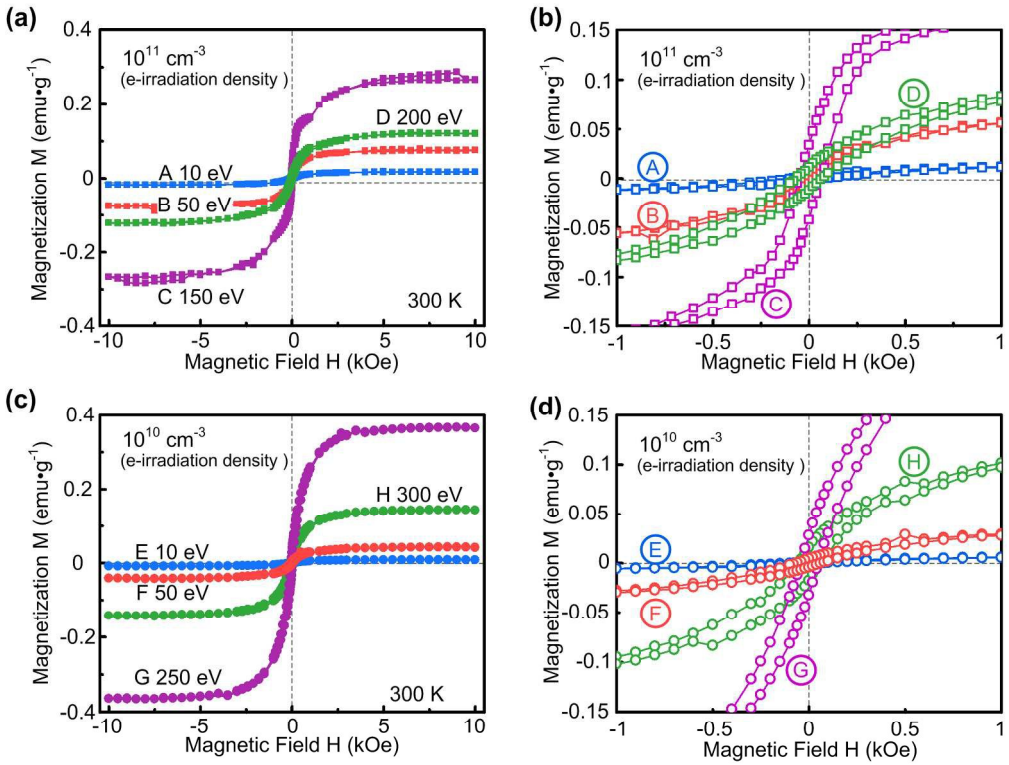

Figure 2

203x167mm (300 x 300 DPI)

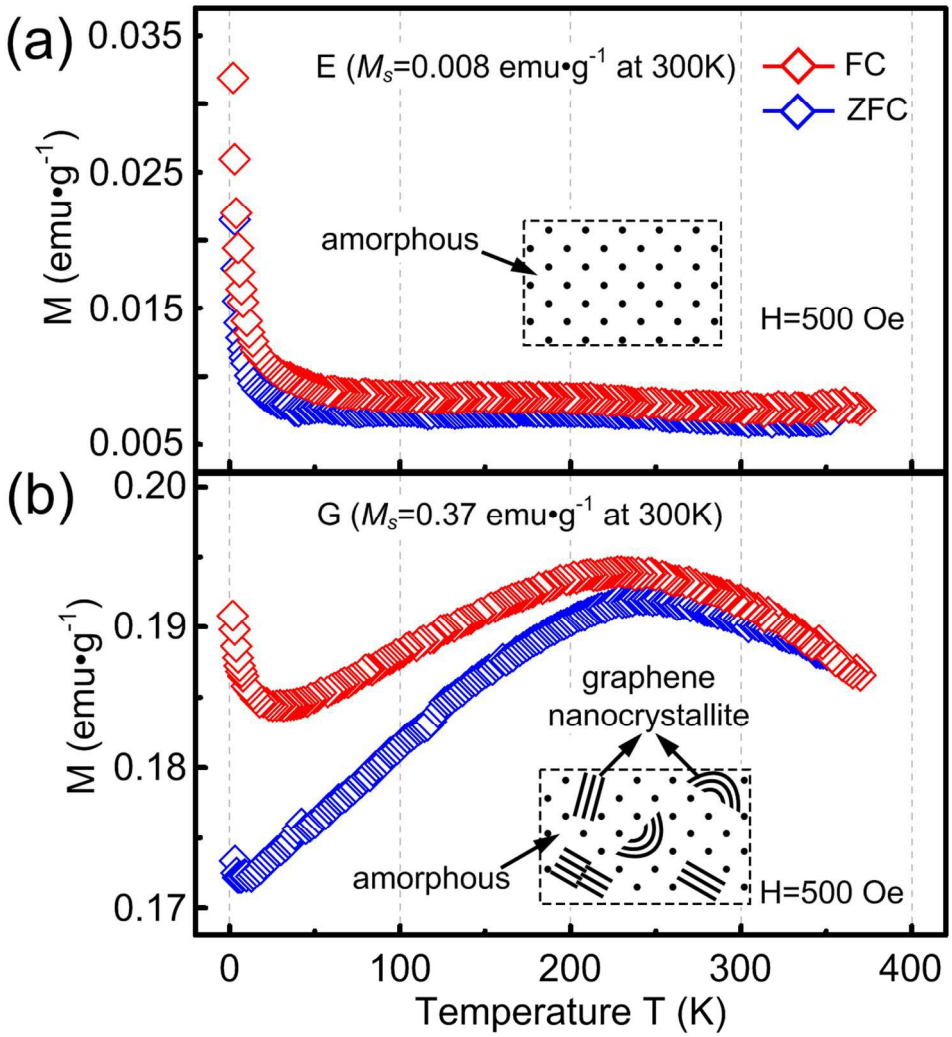

Figure 3

111x127mm (300 x 300 DPI)

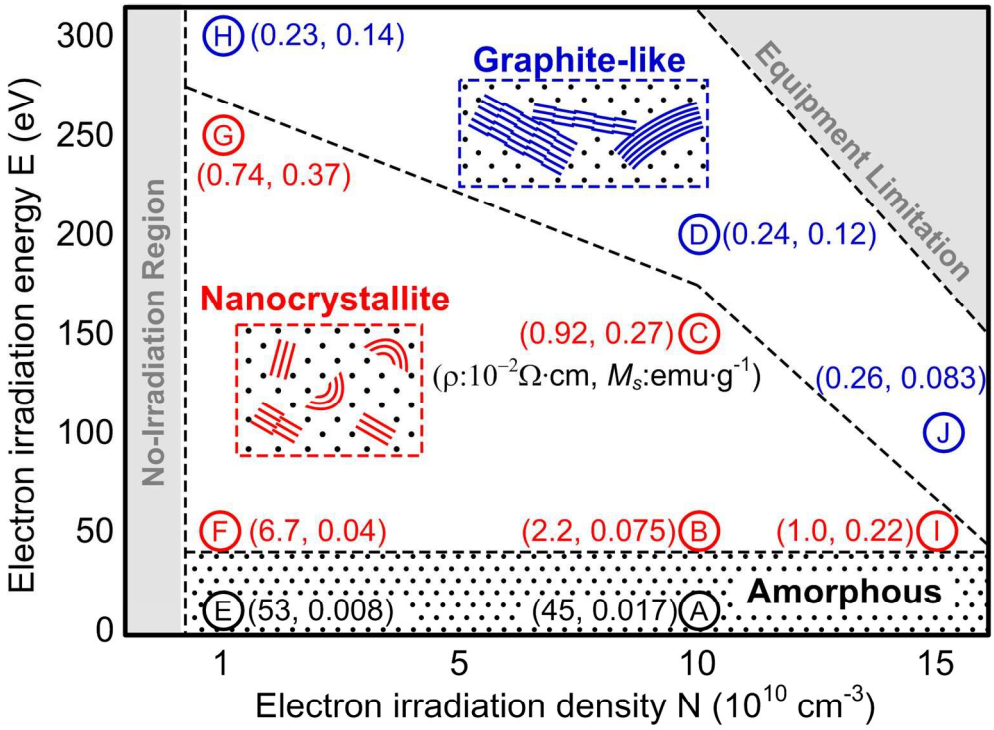

Figure 4

151x120mm (300 x 300 DPI)

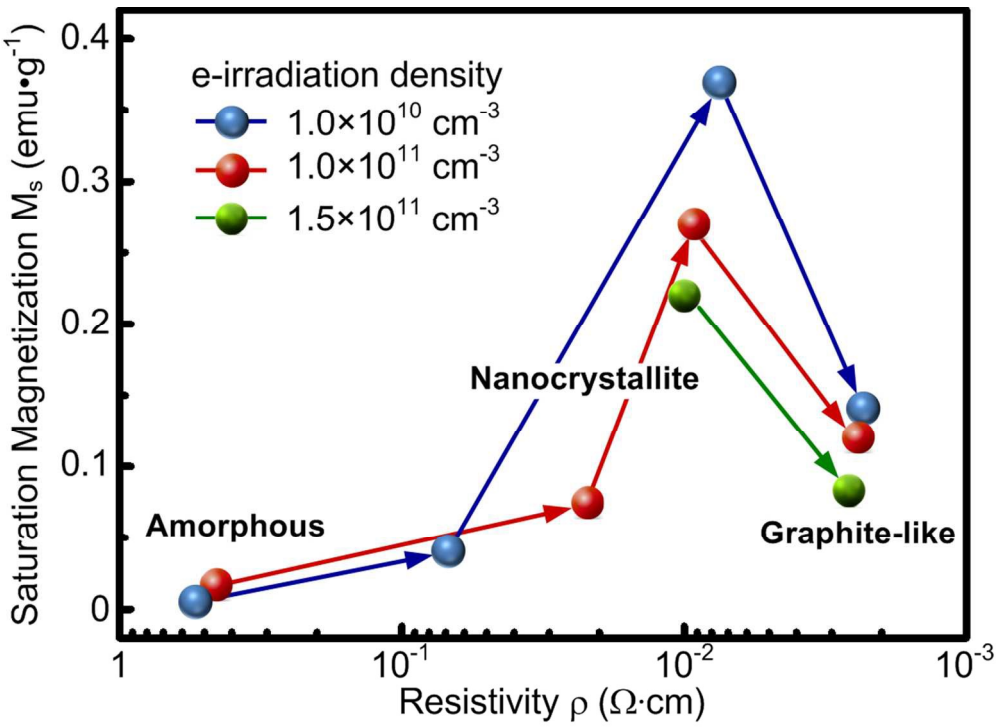

Figure 5

98x83mm (300 x 300 DPI)